

Effects of Configuration Control on the Neoclassical Viscosity in Heliotron-J

Shin NISHIMURA^a, Yuji NAKAMURA^b, Gen MOTOJIMA^a, Hiroyuki OKADA^c,
Shinji KOBAYASHI^c, Satoshi YAMAMOTO^d, Kazunobu NAGASAKI^c,
Kiyoshi HANATANI^c, Katsumi KONDO^b, Tohru MIZUUCHI^c, Fumimichi SANŌ^c

^a National Institute for Fusion Science, Oroshi-cho 322-6, Toki, 509-5292, Japan

^b Graduate School of Energy Science, Kyoto University, Uji, 611-0011, Japan

^c Institute of Advanced Energy, Kyoto University, Uji, 611-0011, Japan

^d Pioneering Research Unit for Next Generation, Kyoto University, Uji, 611-0011, Japan

(Received: 5 September 2008 / Accepted: 12 December 2008)

The three mono-energetic viscosity coefficients are investigated in Heliotron-J as a benchmarking of the analytically approximated formulas of the neoclassical viscosities. One purpose is to validate an analytical theory for the ripple-trapped/untrapped boundary layer in the velocity space even for configurations with arbitrary magnetic field Fourier spectra and large rotational transform per toroidal period. Therefore dependence of the non-diagonal coefficient, which determines spontaneous parallel flows such as the bootstrap current, on configurations, collisionality, and radial electric fields is investigated in detail.

Keywords: neoclassical transport, neoclassical viscosity, spontaneous neoclassical flows, moment equation approach, drift kinetic equation, nonsymmetric toroidal plasma

1. Introduction

In a hierarchical description of toroidal plasmas [1], neoclassical transport theory determines quasi-steady-state components of gyro-phase-averaged distribution functions by Coulomb collisions. Various projects for integrated simulation applying this hierarchical description for helical and stellarator devices are now conducted [2]. A most important requirement for the “layer” of the neoclassical part will be its covering area (plasma parameter range and variation of configurations) and a consistency with other layers rather than accuracy in a specific problem in a limited parameter range and in limited configurations. Motivated design activity of advanced helical devices, experimental studies on neoclassical flows, a framework for the neoclassical transport in general non-symmetric toroidal plasmas, which is favorable for this hierarchical description, has been constructed and tested [3,4]. It is important not only for the helical/stellarator devices but also for tokamaks since the partially broken axisymmetry due to the MHD activity causing additional neoclassical effects is recently considered to be important in relation to the rotational stabilization of the resistive wall mode, and the island physics [4-6]. In this unified theory [3,4], three mono-energetic viscosity coefficients M^* (parallel viscosity against flows), N^* (driving force for parallel flows), and L^* (radial diffusion) are required. For practical applications of this theory such as the integrated simulation system [2] and

configuration optimizations (for e.g., STELLOPT code [7], which is now applied for designing trim coils in the Heliotron-J [8]), faster and easier methods to obtain the three coefficients are required. The drift kinetic equation (DKE) giving them is described in the 3 dimensional (3-D) phase space (poloidal and toroidal angles θ , ζ , and the pitch angle ξ) [3,4]. Various bounce- or ripple-averaging methods, which reduce this dimension substantially, are developed for handling the bounce-averaged bounce center motions of the ripple-trapped particles [9,10] and these methods also should be used appropriately in the unified theory and the integrated simulation including it. For the non-bounce-averaged effects, analytically approximated formulas, which are applicable to arbitrary magnetic field (B) spectra, are derived [11,12]. However, there is the ripple-trapped/untrapped boundary layer in the pitch-angle-space, which causes a coupling effect (collisional trapping/detrapping) between the bounce-averaged bounce center motions and the untrapped particles' non-averaged guiding center motions. As neoclassical predictions due to the break of symmetry, dependence of plasma currents on radial electric fields $E_s \equiv -\partial\Phi/\partial s$ is known [13] in addition to well-known spontaneous determination of the E_s by the ambipolar condition. Exactly speaking, there are two mechanisms for this dependence. One mechanism that was firstly pointed out by Nakajima, et al.[13] is the collisionality dependence of the non-diagonal

author's e-mail: nishimura.shin@hd.nifs.ac.jp

coefficient N^* , and the other is the dependence of this coefficient itself on the E_s . The latter dependence is caused by the boundary layer effect that can be calculated by a complementary use of the analytically approximated solution for the boundary layer structure [14] and the bounce-averaging technique giving the boundary condition for this solution [12]. Although this analytical solution is obtained assuming simple B -field spectra without higher non-axisymmetric harmonic modes $n \geq 2$ in the Fourier expansion $B = \sum B_{nm} \cos(m\theta - nN\zeta)$ and assuming small rotational transform per toroidal period t/N , it was confirmed recently in the National Compact Stellarator Experiment (NCSX) [15] and the Quasi-poloidal Stellarator (QPS) [7,16] that we can apply this solution for more general toroidal configurations [17]. For a purpose to validate this boundary layer theory in cases with large t/N values, however, the t/N value in the QPS was not so large even if its toroidal period number $N=2$ is the smallest one in previously designed devices. Here we present recent calculation examples in the Heliotron-J (H-J)[8] as one of recently designed devices with small toroidal period numbers. Especially for future studies of radial electric field effects on the plasma flows, the non-diagonal coefficient N^* is investigated in detail in this devices with larger t/N values.

2. Magnetic Field in Cases with the Bumpy Ripple Control

The H-J [8,18-20] is a helical axis heliotron with a helical coil with the poloidal and toroidal mode numbers of $(L, N)=(1, 4)$, and major and minor radii of $R=1.3\text{m}$ and $a=0.16\text{m}$. In a viewpoint of a technical interest on the analytical calculations partly including a high aspect ratio approximation $\delta B/B \ll 1$, its aspect ratio R/a is not so small compared with those of the Large Helical Device (LHD, a planer axis helical heliotron with $R/a=6.5$, $N=10$) [2, 21], the NCSX (a quasi-axisymmetric torus with $R/a=4.4$, $N=3$)[15], and the QPS (a quasi-poloidal torus with $R/a=3.3$, $N=2$)[7,16]. It is a relatively high aspect ratio, which is comparable to that of the Wendelstein 7-X (W7-X, a helias type torus with $R/a=10.6$, $N=5$)[10]. However, this device is unique in a pioneering idea adopting a small toroidal period number of $N=4$, which is the recent trend of optimization targeting quasi-isodynamic (omnigenous) configurations [8]. Hereafter, the notations for the \mathbf{B} -field expression in Refs.[3,4,12] are followed, and therefore χ and ψ are the poloidal and toroidal flux, $'=d/ds$ is the radial derivative by the flux surface label s . In this paper, we use the flux surface averaged minor radius $\langle r \rangle$ [m] as this label s . In the H-J, the rotational transform per toroidal period $(\chi'/\psi')/N \approx 0.14$ at a radial position of $(\psi/\psi_{\text{edge}})^{1/2} = 0.5$ (in a standard configuration)

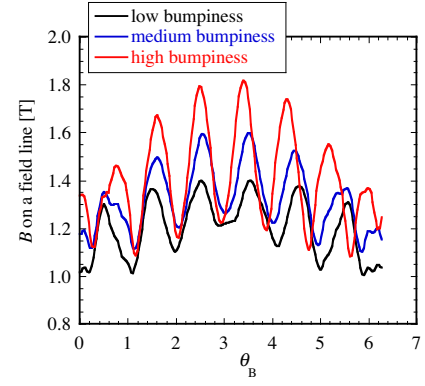


Fig.1 The magnetic field (B) strength on a field line as functions of the poloidal angle θ_B in the Boozer coordinates at radial position of $(\psi/\psi_{\text{edge}})^{1/2} = 0.5$ (corresponding to $\langle r \rangle \approx 0.08\text{m}$) in three configurations in Ref.[20].

parameters	low bumpy $\epsilon_b=0.01$	medium bumpy $\epsilon_b=0.06$	high bumpy $\epsilon_b=0.15$
χ' [Tm]	0.0526879	0.0553847	0.0586983
ψ' [Tm]	0.0949292	0.0998489	0.1087476
B_ζ [Tm]	1.575483	1.708022	1.763566
B_θ [Tm]	3.00×10^{-10}	1.59×10^{-10}	-2.57×10^{-10}
$\langle B^2 \rangle^{1/2}$ [T]	1.189839	1.305393	1.367054
$V/4\pi^2$ [m ²]	0.105642	0.100082	0.102622
H_2	-1.268501	-1.133101	-0.996757

Table 1 The parameters at $(\psi/\psi_{\text{edge}})^{1/2} = 0.5$ as inputs for the viscosity calculation in the next section.

is larger than $(\chi'/\psi')/N \approx 0.096$ in the QPS. (Also in this technical viewpoint on the rotational transform at $(\psi/\psi_{\text{edge}})^{1/2} = 0.5$, the H-J and the W7-X with $(\chi'/\psi')/N \approx 0.16$ have a common characteristic.)

Figure 1 shows the B -field strength on a field line as functions of the poloidal angle θ_B in the Boozer coordinates [3] (s , θ_B , ζ_B) at radial position of $(\psi/\psi_{\text{edge}})^{1/2} = 0.5$. These are configurations used in recent experiments investigating the configuration dependence of the bootstrap (BS) currents [20]: (1) the low bumpiness ($\epsilon_b=0.01$), (2) the medium bumpiness ($\epsilon_b=0.06$), and (3) the high bumpiness ($\epsilon_b=0.15$) configurations. (Following discussions in Ref.[20], we often use here a notation of $\epsilon_b \equiv B_{01}/B_{00}$ at $(\psi/\psi_{\text{edge}})^{1/2} \approx 0.67$ defined by using the Fourier expansion in the Boozer coordinates $B_{nm}^{(\text{Boozer})}$, to represent effects of $m=0, n \neq 0$ Fourier modes in B .) For this kind of situations with higher non-axisymmetric Fourier modes $n \geq 2$ and with large $(N\psi'/\chi' - L)^{-1}$ values making a displacement of the trapping well structure from a simple sinusoidal curve, the conventional analytical methods for the ripple-trapped particle dynamics [22] and the boundary layer equation [14] may be thought to be inappropriate [9,10]. This doubt is due to a fact that

the conventional methods often assume “ideal” model magnetic fields written as $B/B_{00} = 1 + \varepsilon_{\Gamma}(\theta) + \varepsilon_{\text{H}}(\theta) \cos\{L\theta - N\zeta + \gamma(\theta)\}$ with $(N\psi'/\chi' - L)^{-1} \ll 1$. As discussed previously [17], however, we still can apply these theories only with minor modifications in the modeling method of B especially when we calculate the boundary layer correction on the non-diagonal coefficient $N^*_{(\text{boundary})}$ and the $1/\nu^{1/2}$ diffusion effect in the diagonal coefficient $L^*_{(-1/2)}$ since these correction terms are relatively insensitive to the ripple amplitude δ_{eff} . This modeling method is already described in Ref.[17] and thus will not be shown here. In viewpoint of the bounce-averaged radial drift of the ripple-trapped particles, an optimized condition, which is discussed by Mynick, et al. as “ σ -optimization” [23], is approximately realized in the “high-bumpiness” configuration. In fact, well-known $1/\nu$ diffusion component in the diagonal coefficients L^* is reduced in configurations with larger bumpy ripple ($\varepsilon_{\text{b}} \sim 0.1$) in spite of the increased $\varepsilon_{\text{H}}(\theta)$ compared with cases with $\varepsilon_{\text{b}} \leq 0.01$. Similarly to the drift optimizations in QPS[7,16,17], W7-X[10], and the inward shifted configurations in LHD [21], this reduction of the $1/\nu$ diffusion in configurations with larger ripples is one example indicating that it is important to reduce the bounce-averaged radial drift velocity rather than to reduce the fraction of the ripple-trapped particles. An importance of reducing this radial drift velocity is recently stressed again in relation with the zonal flow in non-axisymmetric toroidal plasmas [24]. The parameters including the covariant toroidal and poloidal components of the magnetic field $B_{\zeta}^{(\text{Boozer})}$, $B_{\theta}^{(\text{Boozer})}$ and the radial derivative of the volume enclosed the flux surface $V'/4\pi^2 = (\psi' B_{\zeta} + \chi' B_{\theta}) / \langle B^2 \rangle$ are listed in Table 1. Although the flux-surface-averaged magnetic field strengths and the plasma dimensions are almost identical in these configurations, a constant H_2 differs depending on the bumpy field control. It expresses an effect of the ripple fields on the plasma flow, especially that driven by non-bounce-averaged guiding center motions of deeply trapped particles (with shorter bounce periods), and is defined by [11,12]

$$H_2 \equiv \frac{\langle (\chi' \partial B / \partial \theta_{\text{H}})^2 - (\psi' \partial B / \partial \zeta_{\text{H}})^2 \rangle}{\langle (\chi' \partial B / \partial \theta_{\text{H}} + \psi' \partial B / \partial \zeta_{\text{H}})^2 \rangle} \quad (1)$$

using the Hamada coordinates[3] (s , θ_{H} , ζ_{H}). It is well-known [11,19] that conditions with $H_2 \sim 1$ and $H_2 < -1$ are correspond to nearly axisymmetric $B/B_{00} \equiv 1 + \varepsilon_{\Gamma}(\theta)$ and helically symmetric $B/B_{00} \equiv 1 + \varepsilon_{\text{H}} \cos(L\theta - N\zeta)$ cases, respectively, and that intermediate conditions of $-1 < H_2 \ll 1$ can be seen in configurations where the parallel flow is damped by bumpy fields $B/B_{00} \equiv 1 + \varepsilon_{\text{H}} \cos(N\zeta)$. We can see this tendency in Table.1,

and will show in the next section how the viscosity coefficients depend on this constant.

3. Numerical Examples

Similarly to Refs.[3,12,17], the numerical results for the mono-energetic coefficients M^* , N^* , and L^* in comparisons shown here are obtained using the Drift Kinetic Equation Solver (DKES) [25] together with the conversion formulas Eqs.(43),(54)-(56) in Ref.[3] (and Eq.(41) in Ref.[4]). In collisionality parameters (inverse of mean free path) ν_{D}^a/ν and ν_{T}^a/ν , subscript “D”, “T” indicating collision type and superscript “a” indicating particle species are omitted in figures because these normalized mono-energetic results are those for all species, and the collisionality parameters in the figures means both of the pitch angle deflection ν_{D}^a in collisionless regimes and the pressure anisotropy relaxation $\nu_{\text{T}}^a/3$ in the Pfirsch-Schlüter (P-S) regime where M^* , N^* , $L^* \propto (\nu_{\text{T}}^a/\nu)^{-1}$ [3,12]. Also following these previous works, we show here the non-diagonal coefficient N^* in a normalized form (often called as “geometrical factor” [11,13,19,26]) of $G^{(\text{BS})} \equiv -\langle B^2 \rangle N^*(\nu/\nu, E_s/\nu) / M^*(\nu/\nu)$. In Fig.2, $M^*(\nu/\nu)$ used for this normalization is shown. In a method in Ref.[12] expressing the viscosity coefficients as sum of several components, this factor is given by

$$G^{(\text{BS})} = \psi' B_{\zeta} - \chi' B_{\theta} + \langle B^2 \rangle H_2 \frac{V'}{4\pi^2} - \langle B^2 \rangle \frac{N^*_{(\text{asym})}(\nu/\nu) + N^*_{(\text{boundary})}(\nu/\nu, E_s/\nu)}{M^*(\nu/\nu)} \quad (2)$$

First three terms $\psi' B_{\zeta} - \chi' B_{\theta} + \langle B^2 \rangle H_2 V'/4\pi^2$ express a flow-driving parallel force ($\langle \mathbf{B} \cdot \nabla \cdot \boldsymbol{\pi}_a \rangle$, $\langle \mathbf{B} \cdot \nabla \cdot \boldsymbol{\theta}_a \rangle$) due to non-bounce-averaged guiding center motion of deeply trapped (ripple-trapped in helical/stellarator devices) particles with shorter bounce periods. On the other hand, $N^*_{(\text{asym})}$ expresses effects of barely trapped (toroidally trapped) particles with longer bounce periods, and $N^*_{(\text{boundary})}$ expresses the collisional coupling effect between the toroidally trapped particles and the ripple-trapped particles’ bounce-averaged bounce center motion. Therefore appearances of $N^*_{(\text{asym})}$, $N^*_{(\text{boundary})}$ in $G^{(\text{BS})}$ require sufficiently long mean free path $(\nu/\nu)^{-1}$ for the formation of collisionless trapped orbits with longer bounce periods, and these terms disappear in the collisional limit (P-S regime), $N^*_{(\text{asym})} + N^*_{(\text{boundary})} \approx 0$ at $\nu/\nu \rightarrow \infty$. In this $G^{(\text{BS})}$, only the boundary layer correction term $N^*_{(\text{boundary})}$ is sensitive to ExB drift effects suppressing the well-known $1/\nu$ perturbation in the ripple-trapped pitch-angle range $\kappa^2 < 1$. This term is a monotonically decreasing function of absolute value of the ExB drift parameter $|E_s|/\nu$, and vanishes in a large $|E_s|/\nu$ limit [12]. For electrons, the ExB effects on the neoclassical viscosity coefficients are weak because of

the large thermal velocities ($E_s/v \approx 0$) and thus this term does not vanish even in the experimentally observed conditions with ambipolar radial electric fields of $<10\text{kV/m}$. On the other hand in the energy-integrated coefficients for ions (see Appendix), this term is suppressed by the large $E \times B$ effect of $E_s/v \sim 0.01\text{T}$ in the ambipolar condition. (It also should be noted that there are two different roles of the “radial electric field”. One is that as the $E \times B$ drift parameter E_s/v [3,25] in $N_{(\text{boundary})}^*$ and L^* . These viscosity coefficient are even functions of E_s/v , and therefore we show here only their dependence on $E_s/v \geq 0$. In discussion of the “ E_s -driven flows” in the next section, the radial electric field driving the flows is that as the thermodynamic force X_{a1} defined in Appendix in which the “directions of flows” depend on the sign of E_s .) For this term in the weak radial electric field limit $N_{(\text{boundary})}^*(E_s/v=0)$,

$$N_{(\text{boundary})}^* = -\frac{12}{\pi^2} \frac{v_D^a}{v} \frac{\langle B^2 \rangle}{\chi' \psi' f_c} \frac{V'}{4\pi^2} \times \int_0^\pi d\theta_B \sqrt{2\delta_{\text{eff}}} (\pi - 2\sin^{-1}\alpha^*) \theta_B \left(\frac{\partial \varepsilon_T}{\partial \theta_B} - \frac{2}{3} \sqrt{1-\alpha^{*2}} \frac{\partial \varepsilon_H}{\partial \theta_B} \right) \quad (3)$$

in Ref.[12] is used in this paper, which uses the Shaing-Hokin theory [22] (with replacing the ripple amplitude ε_H by the effective ripple-wall depth δ_{eff} defined in Ref.[17]) for a boundary condition in the boundary layer analysis [14]. To confirm a validity of this use, we show in Fig.3 also L^* in the configuration of $\varepsilon_b=0.06$, which is analytically obtained by the Shaing-Hokin $1/v$ regime theory. Similarly to the calculation example in the QPS [17], this analytically approximated solution retains an accuracy of a factor of 2 even for this coefficient of $\propto(\delta_{\text{eff}})^{3/2}$ in the three H-J configurations, and thus we can investigate the boundary layer correction by applying this solution. Exactly speaking, a sum of contributions of non-bounce-averaged guiding center motions (given by Eq.(16) in Ref.[12]) and the $1/v$ regime asymptotic value $L^*_{(-1)}$ given by the bounce-averaging methods [9,10,22] cannot reproduce exactly the numerically obtained L^* in the transient region between the $1/v$ and plateau regimes (for e.g., $v/v \sim 10^{-2}\text{m}^{-1}$ in the H-J). Although a more exact calculation of this region requires the $1/v^{1/2}$ component $L^*_{(-1/2)}$ and the other boundary layer correction $L^*_{(\text{boundary})}$ [12,17], this problem is out of scope here. Since these corrections to L^* also are caused by the ripple-trapped/untrapped boundary layer, we have to validate the boundary layer theory [14] firstly in the non-diagonal coefficients N^* in which the boundary layer correction clearly (not transiently) appears in a wide range of collisionality in collisionless limit with weaker $E \times B$ drift effects $E_s/v \approx 0$. It also should be noted on cases with finite $E \times B$ drift $E_s/v \neq 0$ in multi-helicity

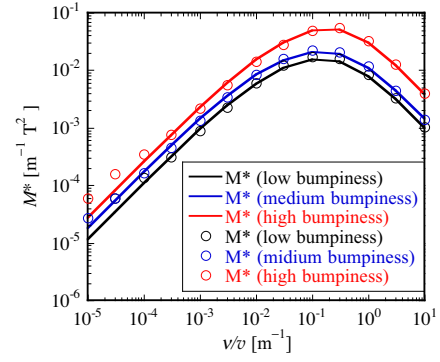


Fig.2 The diagonal mono-energetic coefficient expressing the parallel viscosity against flows M^* given by the analytical formula (solid curves) and the numerical calculation with the DKES (open circles) at radial position of $(\psi/\psi_{\text{edge}})^{1/2}=0.5$ in three configurations.

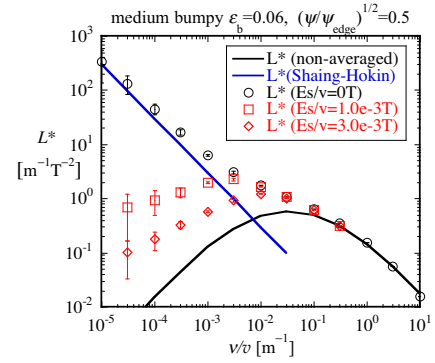


Fig.3 The diagonal mono-energetic coefficient L^* (radial diffusion) given by the analytical formulas and the DKES (open symbols). The analytical calculation includes two parts, a contribution of non-bounce-averaged motions given by Eq.(16) in Ref.[12] (black solid curve) and that of the bounce-averaged motion of the ripple-trapped particles given by the Shaing-Hokin theory [22] (blue solid line).

configurations [17] that the $v^{1/2}$ regime of L^* appears in wide ranges of the collisionality instead of collisionless detrapping “ v regime”. The scaling of $L^* \propto (v/v)/(E_s/v)^2$ in Ref.[27] is valid only in so-called single-helicity configurations such as an example in Fig.5 in Ref.[12] or in more collisionless limits in general configuration. Another important purposes to compare the analytical formulas and the numerical calculations for N^* is to clarify this (v/v , E_s/v) range where the previous banana regime theory by Shaing, et al.[11] is valid. Since they neglected the boundary layer correction term $N_{(\text{boundary})}^*$ in Eq.(2), their theory must be interpreted as an expression for a limit with appropriately strong radial electric field $E_s/v \neq 0$ where the $1/v$ perturbation is suppressed.

Figure 4 shows the geometrical factor $G^{(\text{BS})}$. Similarly to Refs.[3,4,11,13], the sign of $G^{(\text{BS})}$ (and/or N^*) is defined as follows. For the spontaneous parallel flows driven by normal pressure gradients $\partial p_a/\partial s < 0$, $G^{(\text{BS})} > 0$ indicates the BS current generation in co-direction (ion flow velocity in co-direction and electron flow velocity in

counter-direction). For the flows driven by positive radial electric fields $E_s > 0$, $G^{(BS)} > 0$ generates flow velocities in co-direction for both of ions and electrons. In pure non-bounce-averaged effects excluding the $N_{(\text{boundary})}^*$, it can be seen that the configuration dependence in the H-J is mainly that of the first three terms in Eq.(2) including the constant H_2 in Eq.(1). The values of $\psi' B_\zeta - \chi' B_\theta + \langle B^2 \rangle H_2 V' / 4\pi^2$ in the low-, medium-, and high-bumpiness configurations are -0.04016 , -0.02270 , and 6.22×10^{-4} , respectively. This dependence, in which the large bumpy ripple reduces the BS-current in counter-direction generated by effects of deeply trapped

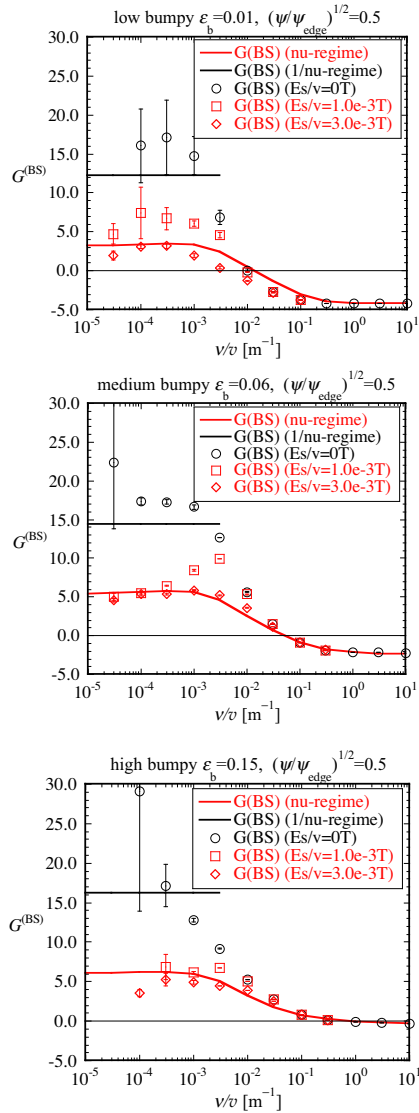


Fig.4 The geometrical factor $G^{(BS)} \equiv -\langle B^2 \rangle N^* / M^*$. In the analytical results shown by red solid curves, the boundary layer correction in the $1/\nu$ regime in Eq.(3) is omitted and therefore they correspond to conditions with sufficiently large $E \times B$ parameter E_s/v ($\approx 10^{-3}T$) in which the $1/\nu$ diffusion in Fig.3 is suppressed. Black solid lines indicate $1/\nu$ regime asymptotic values given by adding Eq.(3). The DKES results are indicated by open symbols for both of the $1/\nu$ regime ($E_s/v=0$) and the ν (or $\nu^{1/2}$) regime ($E_s/v \approx 10^{-3}T$).

particles, is qualitatively consistent with recent experimental observation [20] where larger BS-currents in co-direction were observed in configurations with larger large bumpy ripple. Since the bootstrap currents are determined by using the energy-integrated viscosity coefficients as shown in Appendix, this experimentally observed increase of the currents in the co-direction means also a decrease of contributions of low energy particles (in range of $v < v_{Ta}$) with high collisionality $\nu(v)/v > 10^{-1}m^{-1}$, which make the current-driving forces in counter direction, in the integration $\int dK$. However, this present calculation is quantitatively different from the previous analysis in Ref.[20] as discussed in the next section. The dependence of the DKES results with $E_s/v \approx 10^{-3}T$ indicates that the formulas derived by Shaing, et al.[11] expresses both of the ν and $\nu^{1/2}$ regimes, although this fact was not stated in Ref.[12] that investigated mainly a single-helicity configuration.

4. Discussion and Conclusion

Because of a problem on the collisional momentum conservation stated in Ref.[11], this kind of quantitative benchmarking tests of the non-diagonal coefficient N^* had not been reported before the work in Ref.[3]. Therefore we recently concentrated in testing theories of N^* after Ref.[3] that clarified a relation between the previous analytical theories for the flows [11,13] and the numerical methods for the DKE [21,25]. A consistency of the new unified theory in Refs.[3-4], which fully includes the previous theories in Refs.[11,13] as a strong radial electric field limit ($E_s/v \rightarrow \infty$), have been confirmed by these studies. For the boundary layer correction $N_{(\text{boundary})}^*$, which was neglected in the previous analytical theories [11,13], it is demonstrated that a complimentary use of the bounce- or ripple-averaging methods together with the analytical solution for the boundary layer structure [14] will be usable in practical applications. In Ref.[17] and the present study, however, we investigated only the $1/\nu$ regime ($\nu/v, E_s/v \rightarrow 0$) asymptotic value in Eq.(3). It will be important for the practical applications to make a formula for the $\nu/v, E_s/v$ dependence of $N_{(\text{boundary})}^*(\nu/v, E_s/v)$ in Eq.(2) which smoothly connects this asymptotic value to the plateau and the ν (or $\nu^{1/2}$) regimes. Although a basic idea for this connection formula in the single-helicity configurations is shown in Ref.[12], the scaling of $L^{*(\nu)} \propto (\nu/v)/(E_s/v)^2$ [27] assumed there is not generally valid [17]. Therefore the connecting method applicable for general multi-helicity configurations still remains as future theme and will be reported elsewhere.

Nevertheless, we can discuss here some relations of present calculation results for N^* with past preliminary analyses using previous BS current codes (called SPBSC or BSC) [19,26] for recent H-J experiments [20].

By comparing Fig.2 and Fig.4, we can see that the collisionality of the transient regime $v/v \sim 10^{-2} \text{m}^{-1}$ in $G^{(\text{BS})}$, where the collisional limit value $G^{(\text{BS})} \equiv \psi' B_\zeta - \chi' B_\theta + \langle B^2 \rangle H_2 V' / 4\pi^2$ and the collisionless limit value including finite $N^* (\text{asym}) + N^* (\text{boundary})$ are connected, is different from that of the plateau regime of M^* ($M^* \propto (v/v)^0$ at $v/v \sim 10^{-1} \text{m}^{-1}$). In contrast to this collisionality regime boundary of $G^{(\text{BS})}$ (or $N^* (\text{asym}) + N^* (\text{boundary})$) determined by the toroidally tapping effects as mentioned on Eq.(2), that of M^* is determined mainly by the ripple-trapping effects. However, the connection formula in the previous codes assumed that the collisionality regime boundary $G^{(\text{BS})}$ is that of M^* [26]. It is a shortcoming of an inappropriate analogy of tokamaks, and the formula neglects a fact that there are two types of flow-driving mechanisms due to the ripple-trapping and the toroidally trapping in helical/stellarator configurations [12]. Therefore, in the plasma parameter range corresponding to the ‘‘plateau’’ regime $10^{-3} \text{m}^{-1} < v/v < 10^{-1} \text{m}^{-1}$, these previous codes often result in overestimations of the BS current in co-direction. So far, the collisionality dependence of the BS current in the H-J was investigated by density scan experiments, and the theoretical predictions were often larger than the measured values in medium density plasmas with spontaneous current component in co-direction [20]. A main cause of this discrepancy is an inappropriate connection formula. Another discrepancy was pointed out in an extremely low-density limit of $n_e \sim 0.4 \times 10^{19} \text{m}^{-3}$. When the mean free path of ions is not so long ($v_i/v_i > 10^{-2} \text{m}^{-1}$), the flow direction of ion driven by positive radial electric fields $E_s > 0$ can be in counter-direction ($G_i^{(\text{BS})} < 0$) especially in the low bumpiness configuration ($\epsilon_b \approx 0.01$). On the other hand, the electron collisionality is in relatively long mean free path regime ($v_e/v_e < 10^{-2} \text{m}^{-1}$) in the ECH plasmas [20] and thus the E_s -driven electron flow tends to be in co-direction because of $G_e^{(\text{BS})} > 0$. This difference of the collisionality and resulting difference of $G_a^{(\text{BS})}$ between particle species generates the E_s -driven BS currents [13]. (Exactly speaking, the direction of the flow velocities of each particle species is not determined by $G_a^{(\text{BS})}$ of the individual particle species only, but by the parallel force balance equation coupling the all species [3,4,11,13].) Although detailed plasma parameters (T_e , T_i , E_s) were not reported in Refs.[18-20], following past studies in other medium-sized devices [28], it will be appropriate for the low density ($n_e \sim 0.4 \times 10^{19} \text{m}^{-3}$) ECH plasmas to assume this large difference of the collisionality between particle species and the positive radial electric field of a few kV/m \sim 10kV/m. Therefore the E_s -driven BS current in the counter-direction is expected. As mentioned previously, the boundary layer correction term Eq.(3)

remains in the energy-integrated coefficients N_{ej} for electrons even in this situation. Because of two reasons, the previous BS current codes [19,26] result in an underestimation of the difference $G_e^{(\text{BS})} - G_i^{(\text{BS})}$ in this experimental condition in Ref.[20]. One is aforementioned inappropriate connection formula making overestimation of E_s -driven ion flow in co-direction in conditions with $v_i/v_i \sim 10^{-2} \text{m}^{-1}$. Another reason is the neglect of Eq.(3) for the electrons. It was reported in Ref.[20] that the previous codes required too strong positive radial electric field to explain the BS current in counter-direction observed in the low bumpiness configuration. This discrepancy can be interpreted as the underestimation of $G_e^{(\text{BS})} - G_i^{(\text{BS})}$. In addition to this kind of analyses of the experimental results [18-20], the integrated simulations utilizing iterative calculations of the MHD equilibrium and the transport [1,2], and designing trim coils with the Levenberg-Marquardt algorithm [7] also are important future application areas of this present study.

Acknowledgements

A coordinated research program of the National Institute for Fusion Science (NIFS) NIFS06KUH007 supported this collaboration of NIFS and Kyoto University.

Appendix Bootstrap Current given by the Parallel Force Balance Equation

In this Appendix, we summarize a main result of the parallel force balance equation relating to the bootstrap current. For this calculation after obtaining the mono-energetic coefficients M^* and N^* , we have to calculate the energy-integrated coefficients M_{aj} and N_{aj} with $j=0,1,2$ for particle species $a=e,i$ defined by

$$\begin{aligned} [M_{aj}, N_{aj}] = & \frac{2n_a}{\sqrt{\pi}} \int_0^\infty dK \sqrt{K} e^{-K} \left(K - \frac{5}{2} \right)^{j-1} m_a v_{Ta} K^{3/2} \\ & \times \left[M^*(v(v)/v), \frac{c}{e_a} N^*(v(v)/v, E_s/v) \right] \end{aligned} \quad (\text{A.1})$$

The notations in Ref.[3] are followed here and thus the normalized particle energy

$$K \equiv \left(\frac{v}{v_{Ta}} \right)^2 \equiv \frac{m_a v^2}{2T_a}$$

is used. By solving the force balance equation with these coefficients using a procedure described in Appendix C of Ref.[3], the bootstrap current in a single ion species plasma is given by

$$\begin{aligned}
 J_E^{(BS)} &\equiv J_E - J_E^{cl} \\
 &= n_e e \langle B(u_{\parallel i} - u_{\parallel e}) \rangle / \langle B^2 \rangle^{1/2} - \sigma_S \langle BE_{\parallel} \rangle / \langle B^2 \rangle^{1/2} \\
 &= L_{E1}^e X_{e1} + L_{E2}^e X_{e2} + L_{E1}^i X_{i1} + L_{E2}^i X_{i2} + L_{EE} \langle BE_{\parallel} \rangle / \langle B^2 \rangle^{1/2}
 \end{aligned} \quad (A.2)$$

Here, X_{a1} and X_{a2} are radial gradient forces written as derivatives with respect to the label of the flux surfaces s ,

$$X_{a1} \equiv -\frac{1}{n_a} \frac{\partial p_a}{\partial s} - e_a \frac{\partial \Phi}{\partial s}, \quad X_{a2} \equiv -\frac{\partial T_a}{\partial s}. \quad (A.3)$$

The classical inductive current $J_E^{cl} \equiv \sigma_S \langle BE_{\parallel} \rangle / \langle B^2 \rangle^{1/2}$ determined by the classical Spitzer conductivity σ_S is separated here. The remaining part includes transport coefficients $L_{E1}^e, L_{E2}^e, L_{E1}^i, L_{E2}^i$ and L_{EE} , which are determined by the viscosity coefficients describing the configuration effects. These are written as

$$\begin{bmatrix} L_{E1}^e & L_{E2}^e \end{bmatrix} = \frac{n_e e}{\langle B^2 \rangle^{1/2}} [1 \ 0] (\mathcal{M}_e + \Lambda_e)^{-1} \mathcal{N}_e, \quad (A.4)$$

$$\begin{aligned}
 &\begin{bmatrix} L_{E1}^i & L_{E2}^i \end{bmatrix} = \\
 &-\frac{n_e e}{\langle B^2 \rangle^{1/2}} [1 \ 0] (\mathcal{M}_e + \Lambda_e)^{-1} \mathcal{M}_e \begin{bmatrix} 1 & 0 \\ 0 & 0 \end{bmatrix} (\mathcal{M}_i + \Lambda_i)^{-1} \mathcal{N}_i,
 \end{aligned} \quad (A.5)$$

$$L_{EE} = -\frac{n_e e^2 \tau_{ee}}{m_e} [1 \ 0] \left[\Lambda_e^{-1} - (\mathcal{M}_e + \Lambda_e)^{-1} \right] \begin{bmatrix} 1 \\ 0 \end{bmatrix}, \quad (A.6)$$

by using following 2×2 matrices of the energy-integrated viscosity coefficients M_{aj} , N_{aj} , and friction coefficients l_{ij}^{aa} with the small mass ratio approximation for this single ion species case.

$$\mathcal{M}_a = \frac{\tau_{aa}}{n_a m_a \langle B^2 \rangle} \begin{bmatrix} M_{a1} & M_{a2} \\ M_{a2} & M_{a3} \end{bmatrix}, \quad \mathcal{N}_a = \frac{\tau_{aa}}{n_a m_a} \begin{bmatrix} N_{a1} & N_{a2} \\ N_{a2} & N_{a3} \end{bmatrix}$$

$$\Lambda_a \equiv -\frac{\tau_{aa}}{n_a m_a} \begin{bmatrix} l_{11}^{aa} & -l_{12}^{aa} \\ -l_{21}^{aa} & l_{22}^{aa} \end{bmatrix}$$

A qualitative interpretation for Eqs.(A.4)-(A.5) is that the balance of the driving forces $N_{aj} X_{ak}$ and damping forces due to M_{aj} and l_{ij}^{aa} determines the parallel flow velocity $\langle Bu_{\parallel a} \rangle$. The parallel inductive electric field term $L_{EE} \langle BE_{\parallel} \rangle / \langle B^2 \rangle^{1/2}$ is not important in the H-J experiments discussed here [18-20].

Although some conventional theories had been written assuming that $G^{(BS)} = \text{const}$ for all energy (v/v , E_s/v) range [11], this assumption is not generally valid in non-symmetric toroidal plasmas. In the unified theory [3-4] discussed here, this dependence of $G^{(BS)}$ is taken into account by using these 6 integrals in Eq.(A.1). (See also a discussion after Eq.(49) in Ref.[3].)

- [1] A.Fukuyama, et al., in 20th IAEA Fusion Energy Conf. (Villamoura, Portugal, 2004) IAEA-CSP-25/TH/P2-3.
- [2] Y.Nakamura, M.Yokoyama, N.Nakajima, et al., Fusion Sci.Technol. **50**, 457 (2006).
- [3] H.Sugama and S.Nishimura, Phys.Plasmas **9**,4637(2002).
- [4] H.Sugama and S.Nishimura, *ibid.* **15**,042502(2008).
- [5] W.Zhu, et al., Phys.Rev.Lett.**96**, 22002 (2006).
- [6] S.Nishimura, et al., in 21st US TTF Workshop (Boulder, Colorado, USA, March 25-28, 2008) P51.
- [7] D.J.Strickler, et al., Fusion Sci.Technol. **45**, 15 (2004).
- [8] T.Obiki, T.Mizuuchi, et al., Nucl.Fusion **41**, 833 (2001).
- [9] V.V.Nemov, et al., Phys.Plasmas **6**, 4622 (1999).
- [10] C.D.Beidler and H.Maaßberg, Plasma Phys.Contrl.Fusion **43**, 1131 (2001).
- [11] K.C.Shaing, et al., Phys.Fluids B**1**,148(1989).
- [12] S.Nishimura, H.Sugama, and Y.Nakamura, Fusion Sci.Technol. **51**, 61 (2007).
- [13] N.Nakajima, M.Okamoto, and M.Fujiwara, J.Plasma Fusion Res.**68**, 46 (1992).
- [14] K.C.Shaing and J.D.Callen, Phys.Fluids **25**,1012 (1982).
- [15] D.R.Mikkelsen, et al., Fusion Sci.Technol. **51**,166 (2007); H.Neilson, Stellarator News, Issue **115** (June 2008).
- [16] D.A.Spong, S.P.Hirshman, J.F.Lyon, et al.,Nucl.Fusion **45**,918 (2005); J.F.Lyon, B.E.Nelson, R.D.Benson, et al., Fusion Engineering and Design **82**, 575 (2007).
- [17] S.Nishimura, D.R.Mikkelsen, D.A.Spong, et al., Plasma Fusion Res. **3**, S1059 (2008).
- [18] F.Sano, et al., Fusion Sci.Technol. **46**, 288 (2004); H.Okada, et al., J.Plasma Fusion Res. **80**, 883 (2004).
- [19] Y.Nakamura, N.Nakajima, K.Y.Watanabe, and M.Yokoyama, Fusion Sci.Technol. **50**, 281 (2006).
- [20] G.Motojima, et al., Fusion Sci.Technol. **51**, 122 (2007); Nucl.Fusion **47**, 1045 (2007).
- [21] S.Murakami, et al., Nucl.Fusion, **42**, L19 (2002).
- [22] K.C.Shaing and S.A.Hokin, Phys.Fluids **26**, 2136 (1983).
- [23] H.E.Mynick, et al., Phys.Rev.Lett. **48**, 322 (1982).
- [24] H.Sugama and T.-H.Watanabe, Phys.Rev.Lett.**94**,115001 (2005); H.E.Mynick and A.H.Boozer, Phys.Plasmas **14**, 072507 (2007).
- [25] W.I.van Rij and S.P.Hirshman,Phys.Fluids B**1**,563(1989).
- [26] K.Y.Watanabe, et al., Nucl.Fusion **35**,335(1995).
- [27] E.C. Crume, Jr., et al., Phys. Fluids **31**,11(1988).
- [28] S.Nishimura, et al., Fusion Sci. Technol.**46**,77 (2004).